



BSc thesis  
APPLIED MATHEMATICS  
&  
APPLIED PHYSICS

“Particle models for sand transport in water: analysis and simulations”

STEFAN DE GIJSEL

Delft University of Technology

**Supervisors**

Prof.dr. A.W. Heemink

Prof.dr. D.J.E.M. Roekaerts

**Committee members**

Dr. M.B. van Gijzen

Dr. S.R. de Roode

June, 2018

Delft

# Contents

<b>Abstract</b>	<b>iii</b>
<b>1 Introduction</b>	<b>1</b>
<b>2 Theoretical background</b>	<b>2</b>
2.1 Advection-diffusion processes . . . . .	2
2.2 Stochastic processes . . . . .	3
2.3 Fokker-Planck equation . . . . .	4
<b>3 Particle models for simulation of sand transport and corresponding PDEs</b>	<b>5</b>
3.1 Random walk model . . . . .	5
3.2 Random flight model . . . . .	6
3.3 Particle deposition . . . . .	7
3.4 Particle suspension . . . . .	8
3.5 Particle interaction . . . . .	8
3.5.1 Deriving a PDE for $HC$ . . . . .	9
3.5.2 Deriving a PDE for the mass expectation . . . . .	10
3.5.3 Deriving a PDE for the second moment of mass using non-central moments	11
3.5.4 Deriving a PDE for the second moment of mass using central moments . .	12
3.5.5 Solving the system for a Gaussian mass distribution . . . . .	13
3.5.6 System of equations for a general function $g(HC, m)$ . . . . .	14
3.5.7 Finding a suitable function $g(HC, m)$ . . . . .	14
3.5.8 Final system of equations . . . . .	15
3.5.9 Comparison with currently used interaction equations . . . . .	15
<b>4 Numerical simulations of the various particle models</b>	<b>17</b>
4.1 Test environments . . . . .	17
4.1.1 $H = 10$ , $U = V = 0$ , and $D$ a 2D Gaussian curve . . . . .	17
4.1.2 $U = V = 0$ , $D = 10$ , and $H$ a smooth curve with two levels . . . . .	18
4.1.3 $H = 10$ , $D = 10$ , and $U, V$ such that the water rotates divergence-free . . .	19
4.2 Random walk model & random flight model . . . . .	19
4.3 Random walk model & random flight model with deposition and suspension . . . .	23
4.4 Random walk model without & with particle interaction . . . . .	26
<b>5 Conclusions and recommendations</b>	<b>28</b>
<b>References</b>	<b>30</b>
<b>Appendix A: Third non-central moment of the normal distribution</b>	<b>31</b>

## Abstract

This thesis describes how the simple random walk particle model can be extended to account for sand deposition and suspension, and for particle interaction: clumping together and falling apart. The extended models are analyzed, and the corresponding partial differential equations are derived. These equations are compared to the currently used transport equations. The majority of the analysis is about particle interaction, for which a stochastic differential equation for mass was added to the random walk model. The resulting equation for the particle number density is not in complete agreement with the one that is currently used, due to the choice of the mass equation.

Furthermore, numerous simulations are done using both the basic models and the extended ones. The simulation results were as expected. Several comparisons are made between the random walk model and the random flight model, and between models with and without the extensions described. For these comparisons too, the results were as expected.

Recommendations for further research include simulating with more realistic conditions and domains, and developing a more advanced model extension for particle interaction. Also, the effects of particle interaction on particle deposition and suspension could be analyzed, as this thesis does not cover an extended model for both effects.

# 1 Introduction

These days, it is becoming ever more important to predict how particles in water behave. We want to know where plastics in oceans float to, but also how sand moves from one place to another on the bottom of a river. Much research has been done, but there is still a lot to be learned as well. One way to predict the behavior of particles is by solving transport equations, resulting in a function of concentration depending on position and time. This is, however, not always practical. For example, when we want to account for particle interaction (particles clumping together, or falling apart), these equations tend to become very complex and hard to solve.

A different approach is to simulate the behavior of individual particles, using so called particle models. The movements and behavior of a relatively small amount of particles can be simulated and tracked individually. With this information, predictions can be made concerning the enormous amounts of particles we are actually interested in.

The specific particle of interest in this research is sand. It has got some unique properties: sand particles can sink and settle at the bottom of the water, and whirl up again due to the current. Also, sand particles can come together and form one new particle that is heavier. In this bachelor thesis, two well known models are extended such that they can describe these effects. The models are then analyzed, compared to the currently used equations for concentration, and furthermore, various simulations are done using these models.

The particle models are not just very important to predict the behavior of sand, they can also be used to describe all different kinds of particles in numerous sorts of water. Plastics have been named earlier - the need of reliable position predictions of plastic particles has never been as high as now. Models such as the ones described in this project could, with some modifications, easily be used to deliver those predictions. This underlines the importance and versatility of particle models.

This report is built up as follows: in chapter 2, the theoretical background, that is needed to understand the analysis of the models, is covered. Then, in chapter 3, the basic models are given and explained, including the extensions. In the next chapter, 4, these models are used to run simulations, and the results are analyzed. Finally, chapter 5 contains the conclusions that can be drawn from the research, and some discussion points, as well as recommendations for comparable and follow-up research.

## 2 Theoretical background

In order to better understand the particle models that are treated in this report, it is useful to have an overview of the theory behind these models. This theory includes the advection-diffusion equation, stochastic differential equations, and Fokker-Planck equations.

### 2.1 Advection-diffusion processes

In this report, all processes described are advection-diffusion processes. This means that particles can move due to two factors: advection and diffusion.

In this project, we are looking at sand particles in water. When water flows, particles in the water are 'dragged along' with it. The transport of particles due to this water flow is called advection. How large the effect of advection is, is dependent on the water velocity. With this velocity, we mean the velocity at large scales. If the depth of the water is not constant, the rate at which this depth changes also influences the advection process.

But there is something else that causes transport: imagine dropping some ink in a glass of water. The water has absolutely no velocity, and the depth of the water is constant. Still, the ink will slowly spread out, until it is uniformly distributed over the water. This process is called diffusion. The cause of diffusion is the movement of molecules (which is at the basis, of course, also the cause of advection). A particle is pushed around by the surrounding molecules, and due to this pushing, it makes seemingly random movements. This motion is called Brownian motion. When we look at a lot of particles, or even better, just at concentrations, we see that the particles slowly spread out due to their random motions [6].

To describe both advection and diffusion, we can derive an equation for the concentration  $C$  [kg/m<sup>3</sup>]. To describe the diffusive flux, our starting point is Fick's law [11]:

$$\phi''_{m,x} = -D \frac{\partial C}{\partial x}. \quad (1)$$

This law tells that the mass flux  $\phi''_{m,x}$  [kg/m<sup>2</sup>s] in a direction  $x$ , is proportional to minus the gradient of the concentration in that direction. The minus sign makes sure that the mass transport takes place from high to low concentration. We call the proportionality constant  $D$  [m<sup>2</sup>/s], the diffusion coefficient.

Advective flux is described by the following equation, in which  $v_x$  [m/s] is the flow velocity of the fluid in  $x$ -direction:

$$\phi''_{m,x} = v_x C. \quad (2)$$

To derive a general transport equation that describes both advection and diffusion, we take a look at a little cube in space with dimensions  $dx$ ,  $dy$ ,  $dz$ , as Van den Akker and Mudde describe in their derivation in [11]. The derivation is done with the principle of mass conservation in mind. Due to advection, through the left face of the cube,  $[v_x C]_{x,y,z} dydz$  flows in, and through the right face,  $[v_x C]_{x+dx,y,z} dydz$  flows out. This yields a net transport in the  $x$ -direction of

$$-\frac{\partial(v_x C)}{\partial x} dx dy dz,$$

and equivalent terms for the  $y$ - and  $z$ -direction. Same reasoning applies to diffusion terms: if the diffusion process obeys Fick's law, we have  $-D[\frac{\partial C}{\partial x}]_{x,y,z} dydz$  flowing in through the left face, and  $-D[\frac{\partial C}{\partial x}]_{x+dx,y,z} dydz$  flowing out through the right face. This gives the net transport due to diffusion in the  $x$ -direction:

$$\frac{\partial}{\partial x} \left( D \frac{\partial C}{\partial x} \right) dx dy dz.$$

If there is production in the cube, we can denote it by  $r dx dy dz$ , with  $r$  [kg/m<sup>3</sup>s] the reaction speed. The change in mass in the cube is given by  $\frac{\partial C}{\partial t} dx dy dz$ , so to obtain the total transport equation, we put all terms together, and divide by  $dx dy dz$ :

$$\frac{\partial C}{\partial t} = -\frac{\partial(v_x C)}{\partial x} - \frac{\partial(v_y C)}{\partial y} - \frac{\partial(v_z C)}{\partial z} + \frac{\partial}{\partial x} \left( D \frac{\partial C}{\partial x} \right) + \frac{\partial}{\partial y} \left( D \frac{\partial C}{\partial y} \right) + \frac{\partial}{\partial z} \left( D \frac{\partial C}{\partial z} \right) + r. \quad (3)$$

We call this equation the advection-diffusion equation.

Later in this report, when discussing sand particles that settle at the bottom of the water and whirl up from it, we are actually talking about source and sink terms, denoted by  $r$  in (3). The terms could be dependent on each of the variables that are already present in the equation.

### Disadvantage of predictions using the advection-diffusion equation

Unfortunately, using the advection-diffusion equation to predict concentrations has some disadvantages. Solving the equation numerically (the Eulerian approach) is of course possible, but not too easy. Schemes for approximating the equation may introduce negative concentration in case of high concentration gradients, according to Van Stijn, Praagman and Van Eijkeren in [12]. As will be described in chapter 4, a simulation often starts with all particles at a single point or in a small area. Of course the gradients are then very high, and we might run into trouble.

A different option for predicting concentrations is to use stochastic models. For a finite number of particles, their movement is simulated, and we can draw conclusions from the resulting distribution of the particles. To design such models, we need to understand what stochastic differential equations are.

## 2.2 Stochastic processes

A stochastic differential equation (SDE) is a model for some stochastic process [8]. In our case, the random motion of a particle that is the cause of diffusion, is a process that can only be described in terms of probabilities. Therefore, it is a stochastic process, and we can define a stochastic differential equation to describe it.

The SDEs that are used in the context of this project have the form

$$d\mathbf{X}_t = \mathbf{f}(\mathbf{X}_t, t)dt + \mathbf{g}(\mathbf{X}_t, t)d\mathbf{W}_t. \quad (4)$$

The equation gives the change in the stochastic variable  $\mathbf{X}_t$ , an  $n$ -vector. On the right-hand side, we have two terms: a deterministic term, and a random one. The deterministic term can just be calculated based on the previous value of  $\mathbf{X}_t$  and the value of  $t$ . The random term can also have some deterministic part in it ( $\mathbf{g}$ ), but  $d\mathbf{W}_t$  denotes some random value.  $d\mathbf{W}_t$  is a Wiener process, or Brownian motion. It is a Gaussian random variable with mean zero and variance  $dt$  [8]. Note that  $\mathbf{f}$  is an  $n$ -vector,  $\mathbf{g}$  is an  $n$  by  $m$  matrix, and  $\mathbf{W}_t$  is an  $m$ -dimensional Wiener process. In our case,  $m$  is always equal to  $n$ .

This equation is a so called  $\hat{\text{I}}$ to SDE, as all the SDEs in this project are. This type of SDE has some properties that are useful when doing calculations and derivations with them [8].

In this project,  $\mathbf{X}_t$  describes both the x- and y-position of a particle, and  $d\mathbf{W}_t$  describes Brownian motion. Although the SDE is not term-by-term comparable with the advection-diffusion equation, we have some intuition that the random part of the SDE largely describes diffusion, and the deterministic part the advection.

An important thing to notice, is that the prediction of the next value in the stochastic model does only depend on  $t$  and the value  $\mathbf{X}_t$ . It is not dependent on previous values  $\mathbf{X}_{t-\epsilon}$  ( $\epsilon > 0$ ), which is very practical when using the model. Models that have the property that the prediction of future values only depend on the current value, and not past ones, are called Markov [8].

### 2.3 Fokker-Planck equation

To determine if a stochastic model corresponds to a model described in partial differential equations (this is called consistency), it is useful to derive PDEs from stochastic models. This can be done using the Fokker-Planck equation. An SDE has its own Fokker-Planck equation. For the SDE (4), the corresponding Fokker-Planck equation is

$$\frac{\partial p}{\partial t} = - \sum \frac{\partial [f_i p]}{\partial x_i} + \frac{1}{2} \sum \sum \frac{\partial^2 [(g g^T)_{ij} p]}{\partial x_i \partial x_j}. \quad (5)$$

In our case, where (4) describes particle behavior,  $p = p(x, y, t)$  is a probability density function: it gives us the probability to find a particle at location  $(x, y)$ , at time  $t$ .

To find a stochastic model that is consistent with the advection-diffusion equation, we can rearrange (3) in such a way that we can deduce  $\mathbf{f}$  and  $\mathbf{g}$ . [8]

### 3 Particle models for simulation of sand transport and corresponding PDEs

To describe the movement of sand particles in water, various particle models could be used. Of those models, the random walk model is the best-known and the simplest. The second model that will be discussed is the random flight model. This model should improve the behavior of the sand particles just after being suspended. One important aspect of the behavior of sand particles is that they are subject to deposition and suspension. Also, the particles can interact: they can clump together or fall apart. Both the random walk model and the random flight model are extended with the appropriate deposition and suspension terms. The random walk model is extended with an equation to account for particle interaction.

#### 3.1 Random walk model

We impose a water velocity  $U(x, y)$  in the x-direction, and  $V(x, y)$  in the y-direction. The height of the water column at a certain position is given by  $H(x, y)$ , and  $D(x, y)$  is the horizontal dispersion coefficient. We will assume all these parameters to be constant in time. The displacement of a particle can then be described by the following system of Itô stochastic differential equations [5]:

$$\begin{aligned} dX_t &= \left( U + \frac{1}{H} \frac{\partial(HD)}{\partial x} \right) dt + \sqrt{2D} dW_t^x; \\ dY_t &= \left( V + \frac{1}{H} \frac{\partial(HD)}{\partial y} \right) dt + \sqrt{2D} dW_t^y, \end{aligned} \quad (6)$$

with  $W_t = [W_t^x \ W_t^y]^T$  a vector Brownian motion process. The first right hand side term of each equation describes the - deterministic - drift of the particle, where the second, stochastic term accounts for the random part of the diffusive behavior of the particle. This model is constructed such that it is consistent with the depth integrated advection-diffusion equation. [7]

This depth integrated equation follows from (3), where we now take  $C(x, y, t)$  to be the depth-averaged concentration [ $\text{kg}/\text{m}^3$ ], and  $H(x, y, t)$  the depth [m]. The z-direction terms are of course taken out, and from now on, we call the water velocity in the x-direction  $U(x, y, t)$  and in the y-direction  $V(x, y, t)$ . Furthermore, we will not use any production terms for now, so  $r = 0$ . The resulting depth integrated advection-diffusion equation is

$$\frac{\partial(HC)}{\partial t} = -\frac{\partial(HUC)}{\partial x} - \frac{\partial(HVC)}{\partial y} + \frac{\partial}{\partial x} \left( D \frac{\partial(HC)}{\partial x} \right) + \frac{\partial}{\partial y} \left( D \frac{\partial(HC)}{\partial y} \right). \quad (7)$$

By using the Fokker-Planck equation, we can show that the stochastic model is consistent with (7). To do this, we define the probability density function  $f(x, y; t)$  that describes the distribution of the bivariate Markov process  $t \rightarrow (X(t), Y(t))^T$ :

$$f(x, y; t) = \lim_{\Delta x \downarrow 0, \Delta y \downarrow 0} \frac{P[(x \leq X(t) < x + \Delta x) \wedge (y \leq Y(t) < y + \Delta y)]}{\Delta x \cdot \Delta y}. \quad (8)$$

As explained in the previous chapter,  $f$  denotes the probability to find a particle at position  $(x, y)$ , at time  $t$ . Using (5), we see that  $f(x, y; t)$  satisfies the Fokker-Planck equation

$$\begin{aligned}
\frac{\partial f(x, y; t)}{\partial t} = & -\frac{\partial}{\partial x} \left[ \left( U(x, y) + \frac{1}{H(x, y)} \frac{\partial(H(x, y)D(x, y))}{\partial x} \right) \cdot f(x, y; t) \right] \\
& -\frac{\partial}{\partial y} \left[ \left( V(x, y) + \frac{1}{H(x, y)} \frac{\partial(H(x, y)D(x, y))}{\partial y} \right) \cdot f(x, y; t) \right] \\
& + \frac{\partial^2}{\partial x^2} [D(x, y) \cdot f(x, y; t)] + \frac{\partial^2}{\partial y^2} [D(x, y) \cdot f(x, y; t)] .
\end{aligned} \tag{9}$$

With the realization that, for our particle interpretation, the mass density of particles per unit area [kg/m<sup>2</sup>], at position  $(x, y)$  is given by  $f(x, y; t)$ , and that  $f(x, y; t)$  is related to the depth and depth integrated concentration via

$$f(x, y; t) = H(x, y, t)C(x, y, t),$$

we get to the advection-diffusion equation (7) by simple substitutions in (9). Thus, we proved the consistency of the random walk model with the advection-diffusion equation. [4]

### 3.2 Random flight model

The random walk model does a good job describing the dispersion of the sand particles for long times. To be precise: if a particle has been in the turbulent water flow much longer than a Lagrangian timescale  $T_L$ . However, for shorter times, the random walk model is not accurate. To overcome this issue, we can use the random flight model instead. This model does not only describe the position of the particle, but its velocity as well. This addition was made considering the fact that for times much shorter than  $T_L$ , particles tend to have a velocity that stays approximately the same for each timestep. The model was designed to be again consistent with the advection-diffusion equation [7].

The displacement of a particle is now given by

$$\begin{aligned}
dX_t &= \left( U + \sigma U_t + \frac{1}{H} \frac{\partial(HD)}{\partial x} \right) dt; \\
dU_t &= -\frac{1}{T_L} U_t dt + \gamma dW_t^u; \\
dY_t &= \left( V + \sigma V_t + \frac{1}{H} \frac{\partial(HD)}{\partial y} \right) dt; \\
dV_t &= -\frac{1}{T_L} V_t dt + \gamma dW_t^v.
\end{aligned} \tag{10}$$

$U_t$  and  $V_t$  are, respectively, the (stochastic) velocity of the particle in the x-direction and y-direction, due to the turbulent water flow. We will call them the turbulent velocities from now on.  $\sigma(x, y)$  is some parameter that is dependent of space, and  $\gamma$  is a constant. We assume  $D(x, y)$  to be known, and we take  $\gamma$  to be equal to 1. With the known relation  $D = \frac{1}{2}(T_L \sigma \gamma)^2$ , we can easily calculate  $\sigma$ . [7]

To show that this model is again consistent with the advection-diffusion equation for long times, we note that for these long times,  $\frac{t-t_0}{T_L} \rightarrow \infty$ . We might as well take  $T_L \rightarrow 0$  in the set of stochastic differential equations. Taking this limit, it can be shown that we obtain the following set of Itô equations [7]:

$$\begin{aligned}
dX_t &= \left( U + \frac{D}{H} \frac{\partial H}{\partial x} + \frac{\partial D}{\partial x} \right) dt + \sqrt{2D} dW_t^u; \\
dY_t &= \left( V + \frac{D}{H} \frac{\partial H}{\partial y} + \frac{\partial D}{\partial y} \right) dt + \sqrt{2D} dW_t^v.
\end{aligned} \tag{11}$$

We see that these are exactly the same as the equations for the random walk model, and thus are consistent with the advection-diffusion equation as well.

When using the Fokker-Planck equation, this model gives rise to a new set of partial differential equations for the depth-averaged concentration, as described by Heemink in [7]:

$$\begin{aligned}
\frac{\partial(HC)}{\partial t} &= -\frac{\partial(HUC)}{\partial x} - \frac{\partial(HVC)}{\partial y} - \frac{\partial}{\partial x}(H\sigma\langle u \rangle) - \frac{\partial}{\partial y}(H\sigma\langle v \rangle); \\
\frac{\partial(H\langle u \rangle)}{\partial t} &= -\frac{\partial}{\partial x}(H\sigma\langle u^2 \rangle) - \frac{H\langle u \rangle}{T_L}; \\
\frac{\partial(H\langle v \rangle)}{\partial t} &= -\frac{\partial}{\partial y}(H\sigma\langle v^2 \rangle) - \frac{H\langle v \rangle}{T_L}; \\
\frac{\partial(H\langle u^2 \rangle)}{\partial t} &= -\frac{2H\langle u^2 \rangle}{T_L} + H\gamma^2 C; \\
\frac{\partial(H\langle v^2 \rangle)}{\partial t} &= -\frac{2H\langle v^2 \rangle}{T_L} + H\gamma^2 C.
\end{aligned} \tag{12}$$

The moments that appear in this equations are defined as presented below, where  $p = p(x, y, u, v; t)$  is the probability function corresponding to this problem, like (8) was for the random walk model.

$$\begin{aligned}
\langle u \rangle(x, y, t) &= \int_{-\infty}^{-\infty} \frac{up(x, y, u, v; t)}{H(x, y, t)} dudv; \\
\langle v \rangle(x, y, t) &= \int_{-\infty}^{\infty} \frac{vp(x, y, u, v; t)}{H(x, y, t)} dudv; \\
\langle u^2 \rangle(x, y, t) &= \int_{-\infty}^{\infty} \frac{u^2p(x, y, u, v; t)}{H(x, y, t)} dudv; \\
\langle v^2 \rangle(x, y, t) &= \int_{-\infty}^{\infty} \frac{v^2p(x, y, u, v; t)}{H(x, y, t)} dudv.
\end{aligned} \tag{13}$$

### 3.3 Particle deposition

To add the deposition and suspension of particles to the model, we need to record for each particle whether it is in suspension (in the water) or not (it has settled). We will say  $S_t = 1$  if the particle is in suspension at time  $t$ , and  $S_t = 0$  otherwise. Because we're looking at depth-integrated concentrations, we can not store a height of each particle. Therefore, to determine whether a particle should be deposited, we can only use general probabilities. We use the following expression, as proposed by Charles in [4]:

$$P(S_{t+\Delta t} = 1 | S_t = 1) = 1 - \epsilon\Delta t. \tag{14}$$

Or, in words: the probability that a particle is still in suspension in the next timestep, given that it is in suspension this timestep, is equal to  $1 - \epsilon\Delta t$ . Here,  $\epsilon$  is some constant. It makes sense that the longer the timestep, the smaller the probability that the particle is still in suspension after that timestep: there has been more time for the particle to deposit.

What we actually did, is introducing a new characteristic of the particle: apart from position, and in the flight model, velocity, we now have an extra variable  $S$  that gives information about the particle being in suspension or not. However, we cannot give a stochastic differential equation similar to the ones in (6) for this new variable.

Charles has shown, using a Fokker-Planck equation, that particle deposition gives an extra term  $-\epsilon HC$  in the advection-diffusion equation (7).

### 3.4 Particle suspension

To implement particle suspension, we have to introduce some kind of source term in the model. When thinking about sand particles that 'whirl up' from the bottom of the water, our intuition tells us that this effect is probably dependent on the water speed just above the particle at the bottom. Speed, because it is not dependent on the direction of the water flow if a particle goes into suspension or stays where it was. The water speed is a function of  $U^2 + V^2$ .

Just as for particle deposition, it is not possible to give some extra equation or term in the model that accounts for suspension. The reason for this lies in the fact that in particle models, we follow individual particles. We assume that the bottom of the water forms an unlimited source of new particles. Therefore, it is numerically impossible to follow every particle that is not (yet) in suspension.

An extra equation or term in the model is not possible, but there is a good method to implement particle suspension in simulations. Although most of the implementation aspects for the particle simulations are discussed in chapter 4, it is useful to treat this aspect now. For the used method, the domain is divided into equally sized block-shaped areas - grid cells - for each of which we calculate the expected number of particles to be suspended in that cell, as proposed by Charles in [4]. This number is denoted by  $enp_{(i,j,t)}$  for grid cell  $i, j$  at time  $t$ :

$$enp_{(i,j,t)} = \frac{\Delta x \cdot \Delta y \cdot \Delta t \cdot (U^2 + V^2) \cdot \lambda_s}{M_p}. \quad (15)$$

The expected number of particles to be suspended is obviously linear with the grid cell size ( $\Delta x$  by  $\Delta y$ ) and with the timestep  $\Delta t$ . It is also linear with the total water velocity squared and with the erosion coefficient  $\lambda_s$ , and inversely linear with the mass of the particles to be suspended. The water speed appears squared in this equation, because the shear stress exerted by the water is proportional with the water speed squared, measured just above the particle. [10]

This model could be improved by implementing that no particles are suspended at all, up to a certain water speed. This water speed is called the critical speed, and it is at this speed that just enough shear stress is exerted to suspend the particle. [10] However, it is not the goal of this thesis to describe particle suspension as detailed as possible, and the given model is sufficient for now.

In the same derivation as for particle deposition, Charles showed that suspension comes down to an extra term  $+(U^2 + V^2)\lambda_s$  in the advection-diffusion equation. Including both deposition and suspension, our new depth integrated equation is as follows:

$$\frac{\partial(HC)}{\partial t} + \frac{\partial(HUC)}{\partial x} + \frac{\partial(HVC)}{\partial y} - \frac{\partial}{\partial x} \left( DH \frac{\partial C}{\partial x} \right) - \frac{\partial}{\partial y} \left( DH \frac{\partial C}{\partial y} \right) = -\gamma HC + (U^2 + V^2)\lambda_s. \quad (16)$$

### 3.5 Particle interaction

From now on, to make the equations more readable, we will use the following definitions:

$$\tilde{U} := U + \frac{1}{H} \frac{\partial(HD)}{\partial x}, \quad \tilde{V} := V + \frac{1}{H} \frac{\partial(HD)}{\partial y}.$$

Sediment particles interact: smaller particles can clump together, and a composite particle can fall apart into smaller ones. To account for these interactions, we can add a (coupled) Itô stochastic differential equation, which describes a particle's change of mass, to the basic system of SDEs:

$$dM(t) = g(f(X, Y, t), M(t))dt. \quad (17)$$

Here,  $g$  is an arbitrary function of the mass density  $f(x, y; t)$  [kg/m<sup>2</sup>], and the mass  $M$  [kg]. It depends on its own mass if a particle is likely to fall apart (shrink), or clump together with other particles (grow). Also, it is important how many other particles are around to interact with: for this,  $f(x, y; t)$  is a measure. This mass density  $f(x, y; t)$  is actually equal to the probability density defined in (8), and thus the same as  $HC$ :

$$dM(t) = g(H(X, Y, t)C(X, Y, t), M(t))dt. \quad (18)$$

As a basis, we take the random walk model. The random flight model is only different from the walk model for short times, and for the effects of particle interaction, we are interested in the longer timescales. To get to a new equation that adds particle interaction to the advection-diffusion equation, we aim to construct a partial differential equation for both  $HC$  and the mass expectation  $\langle m \rangle$ , as defined in (24). With these equations, we can make a comparison with the equations that are currently used in sediment research.

To get to the equations, we define a new probability density function as

$$f(x, y, m; t) := \lim_{\Delta x \downarrow 0, \Delta y \downarrow 0, \Delta m \downarrow 0} \frac{P[(x \leq X(t) < x + \Delta x) \wedge (y \leq Y(t) < y + \Delta y) \wedge (m \leq M(t) < m + \Delta m)]}{\Delta x \cdot \Delta y \cdot \Delta m}. \quad (19)$$

Now,  $f(x, y, m; t)$  denotes the probability to find a particle with mass  $m$ , at position  $(x, y)$ , at time  $t$ .

### 3.5.1 Deriving a PDE for $HC$

As  $HC$  is an argument of our function  $g$ , it is important to know what it stands for. We already saw in section 3.1 that  $HC$  is equal to the probability density function  $f(x, y; t)$ , defined for the random walk model. It is important to note that these quantities are in fact also equal to the integral of  $f(x, y, m; t)$  over  $m$ :

$$f(x, y; t) = \int_0^\infty f(x, y, m; t) dm. \quad (20)$$

Now if we think back to the original random walk model, without mass, it must hold that the integral is indeed equal to  $f(x, y; t)$  that we got from the original Fokker-Planck equation (9). As our model is mass conserving, it is clear that adding mass terms to this equation, and then integrating over  $m$  again, gives the same results as having no mass terms at all. So we have  $\int_0^\infty f(x, y, m; t) dm = HC$ .

From (9), we find

$$\frac{\partial(HC)}{\partial t} = -\frac{\partial}{\partial x} [\tilde{U}HC] - \frac{\partial}{\partial y} [\tilde{V}HC] + \frac{\partial^2}{\partial x^2} [DHC] + \frac{\partial^2}{\partial y^2} [DHC]. \quad (21)$$

Using the product rule, we have the following closed equation for  $HC$ :

$$\frac{\partial(HC)}{\partial t} = \left[ -\frac{\partial \tilde{U}}{\partial x} - \frac{\partial \tilde{V}}{\partial y} + \frac{\partial^2 D}{\partial x^2} + \frac{\partial^2 D}{\partial y^2} \right] HC - \tilde{U} \frac{\partial(HC)}{\partial x} - \tilde{V} \frac{\partial(HC)}{\partial y} + D \left[ \frac{\partial^2(HC)}{\partial x^2} + \frac{\partial^2(HC)}{\partial y^2} \right]. \quad (22)$$

### 3.5.2 Deriving a PDE for the mass expectation

With the newly defined  $f(x, y, m; t)$ , the system gives rise to the following Fokker-Planck equation that  $f(x, y, m; t)$  satisfies:

$$\begin{aligned} \frac{\partial f(x, y, m; t)}{\partial t} = & - \frac{\partial}{\partial x} \left[ \left( U(x, y) + \frac{1}{H(x, y)} \frac{\partial(H(x, y)D(x, y))}{\partial x} \right) \cdot f(x, y, m; t) \right] \\ & - \frac{\partial}{\partial y} \left[ \left( V(x, y) + \frac{1}{H(x, y)} \frac{\partial(H(x, y)D(x, y))}{\partial y} \right) \cdot f(x, y, m; t) \right] \\ & + \frac{\partial^2}{\partial x^2} [D(x, y) \cdot f(x, y, m; t)] + \frac{\partial^2}{\partial y^2} [D(x, y) \cdot f(x, y, m; t)] \\ & - \frac{\partial}{\partial m} [g(H(x, y, t)C(x, y, t), m) \cdot f(x, y, m; t)]. \end{aligned} \quad (23)$$

We know that the mass expectation  $\langle m \rangle$  [kg/m<sup>2</sup>] at position  $(x, y)$  and time  $t$  is given by

$$\langle m(x, y, t) \rangle = \int_0^\infty m \cdot f(x, y, m; t) dm. \quad (24)$$

Multiplying the whole equation (23) with  $m \cdot dm$  and integrating over  $m$  gives

$$\begin{aligned} \frac{\partial \langle m(x, y, t) \rangle}{\partial t} = & - \frac{\partial}{\partial x} \left[ \left( U(x, y) + \frac{1}{H(x, y)} \frac{\partial(H(x, y)D(x, y))}{\partial x} \right) \cdot \langle m(x, y, t) \rangle \right] \\ & - \frac{\partial}{\partial y} \left[ \left( V(x, y) + \frac{1}{H(x, y)} \frac{\partial(H(x, y)D(x, y))}{\partial y} \right) \cdot \langle m(x, y, t) \rangle \right] \\ & + \frac{\partial^2}{\partial x^2} [D(x, y) \cdot \langle m(x, y, t) \rangle] + \frac{\partial^2}{\partial y^2} [D(x, y) \cdot \langle m(x, y, t) \rangle] \\ & + \int_0^\infty g(H(x, y, t)C(x, y, t), m) \cdot f(x, y, m; t) dm, \end{aligned} \quad (25)$$

where we interchanged derivatives and integrals in every term. This is only possible because of the assumption that all our functions are smooth enough. For the last term, also integration by parts was used, which is allowed, because we assume that both  $f$  and  $g$  are continuously differentiable functions:

$$\int_0^\infty m \frac{\partial(gf)}{\partial m} dm = mgf \Big|_{m=0}^{m=\infty} - \int_0^\infty gf dm = - \int_0^\infty gf dm.$$

The first term in the middle vanishes because of  $f$  being zero for infinite mass, and  $m$  being zero at  $m = 0$  (obviously).

To evaluate the integral in the last term, we can use the Taylor expansion of  $g$  with respect to  $m$ , around  $\langle m \rangle$ . It makes sense to expand around this point, because we expect all masses to be close to their expected value. Note that the units of  $m$  and  $\langle m \rangle$  are [kg] and [kg/m<sup>2</sup>], respectively. However, we can see  $\langle m \rangle$  as mass when integrating over a control area. Now, we can split the integral in terms with the  $n^{\text{th}}$  moments of  $m$ . The Taylor expansion of  $g$  is

$$g(HC, m) = g(HC, \langle m \rangle) + (m - \langle m \rangle) \frac{\partial g}{\partial m}(HC, \langle m \rangle) + \frac{1}{2} (m - \langle m \rangle)^2 \frac{\partial^2 g}{\partial m^2}(HC, \langle m \rangle) + \dots, \quad (26)$$

which gives the following expression for the integral term, when neglecting the higher order terms, that in (26) are represented by the dots:

$$\begin{aligned} \int_0^\infty g(HC, m) f dm &= \int_0^\infty g(HC, \langle m \rangle) f dm + \int_0^\infty (m - \langle m \rangle) \frac{\partial g}{\partial m}(HC, \langle m \rangle) f dm \\ &+ \frac{1}{2} \int_0^\infty (m - \langle m \rangle)^2 \frac{\partial^2 g}{\partial m^2}(HC, \langle m \rangle) f dm. \end{aligned} \quad (27)$$

Now, we continue the derivation of the distribution of  $m$  by defining higher order moments of the mass distribution. We can do this using non-central moments, or using central moments (which is simpler). Both will be discussed in the upcoming paragraphs.

### 3.5.3 Deriving a PDE for the second moment of mass using non-central moments

We need to define the second non-central moment of the mass:

$$\langle m^2 \rangle = \int_0^\infty m^2 \cdot f(x, y, m; t) dm.$$

Using the fact that  $\int_0^\infty f(x, y, m; t) dm = H(x, y, t)C(x, y, t)$ , the definition of  $\langle m^2 \rangle$ , and the definition of  $\langle m \rangle$ , we get

$$\begin{aligned} \int_0^\infty g(HC, m) f dm &= HC \cdot g(HC, \langle m \rangle) + (\langle m \rangle - \langle m \rangle) \frac{\partial g}{\partial m}(HC, \langle m \rangle) \\ &+ \frac{1}{2} (\langle m^2 \rangle - 2\langle m \rangle^2 + \langle m \rangle^2) \frac{\partial^2 g}{\partial m^2}(HC, \langle m \rangle), \end{aligned} \quad (28)$$

which ultimately leads to the integral

$$\int_0^\infty g(HC, m) f dm = HC \cdot g(HC, \langle m \rangle) + \frac{1}{2} (\langle m^2 \rangle - \langle m \rangle^2) \frac{\partial^2 g}{\partial m^2}(HC, \langle m \rangle). \quad (29)$$

Now, if we plug this into equation (25), we get an equation which is not only dependent of  $\langle m \rangle$ , but also on  $\langle m^2 \rangle$ . To be able to solve for  $\langle m \rangle$ , our goal is to get another equation that is dependent on  $\langle m \rangle$  and  $\langle m^2 \rangle$ , to form a system of two equations with (25). From this system, we should be able to eliminate  $\langle m^2 \rangle$  and solve for  $\langle m \rangle$ , the variable of interest. To get the second equation, we need to repeat the process from (25) to (29), but now starting with multiplication by  $m^2$  to obtain an equation for  $\langle m^2 \rangle$ :

$$\begin{aligned} \frac{\partial \langle m(x, y, t)^2 \rangle}{\partial t} &= - \frac{\partial}{\partial x} \left[ \left( U(x, y) + \frac{1}{H(x, y)} \frac{\partial(H(x, y)D(x, y))}{\partial x} \right) \cdot \langle m(x, y, t)^2 \rangle \right] \\ &- \frac{\partial}{\partial y} \left[ \left( V(x, y) + \frac{1}{H(x, y)} \frac{\partial(H(x, y)D(x, y))}{\partial y} \right) \cdot \langle m(x, y, t)^2 \rangle \right] \\ &+ \frac{\partial^2}{\partial x^2} [D(x, y) \cdot \langle m(x, y, t)^2 \rangle] + \frac{\partial^2}{\partial y^2} [D(x, y) \cdot \langle m(x, y, t)^2 \rangle] \\ &+ 2 \int_0^\infty m \cdot g(H(x, y, t)C(x, y, t), m) \cdot f(x, y, m; t) dm, \end{aligned} \quad (30)$$

in which the last term can be determined using the same method as before:

$$\begin{aligned} 2 \int_0^\infty m \cdot g(HC, m) f dm &= 2\langle m \rangle g(HC, \langle m \rangle) + 2(\langle m^2 \rangle - \langle m \rangle^2) \frac{\partial g}{\partial m}(HC, \langle m \rangle) \\ &+ (\langle m^3 \rangle + \langle m \rangle^3 - 2\langle m^2 \rangle \langle m \rangle) \frac{\partial^2 g}{\partial m^2}(HC, \langle m \rangle). \end{aligned} \quad (31)$$

Here, the third non-central moment  $\langle m^3 \rangle$  is defined analogously to  $\langle m^2 \rangle$ . Now, combining (30) and (31), we get an equation that is not only dependent on  $\langle m \rangle$  and  $\langle m^2 \rangle$ , but as well on  $\langle m^3 \rangle$ . It is clear that repeating this process for higher moments of  $m$  will again give us terms with moments one higher than the previous, and we run into a closure problem. Possible ways to solve this are:

1. Assume that the distribution of  $m$  is Gaussian. Then we can derive a relation between the third non-central moment of  $m$  and the first and second one:  $\langle m^3 \rangle = 3\langle m \rangle \langle m^2 \rangle - 2\langle m \rangle^3$ . The derivation is given in the Appendix. Using this, our system of two equations is only dependent on the first and second moment of  $m$ , and we can ultimately solve for  $\langle m \rangle$ . The third and higher moments are all dependent on the first two moments. Expressing the third moment in the first two as explained above gives exactly the same results as repeating the process of the previous pages up to a higher moment and then express the higher moments in the first two.
2. Assume that some  $n^{\text{th}}$  moment of  $m$  is zero. It should be obvious that the system of equations then only contains  $n - 1$  equations with the same amount of unknown moments of  $m$ , which is solvable. But because our moments are taken around 0, and the distribution function of  $m$  lies completely to the right of 0 (for obvious reasons), the moments of  $m$  only get larger with increasing  $n$ . Therefore, this is not an assumption we want to make.
3. Assume that the distribution of  $m$  is multimodal Gaussian, for example bimodal. As suggested by Verney, Lafite, Brun-Cottan, and Le Hir in [13], simulations with particle models that include interaction show that the resulting distribution of  $m$  can have the form of two peaks: one for lower mass and one for higher mass. A good approximation for this would be the bimodal Gaussian distribution. However, finding the corresponding moments for such a distribution is not easy, certainly not the raw ones. Because higher order moments have to be looked at, cutting off the Taylor expansion in (26) at the second derivative term is not allowed. Analysis of such bimodal distributions should make clear if and when we can cut off the Taylor expansion and set the moments of a certain order and higher to be zero.

Option 3 is considered to be too complicated for this project, but doing this would certainly give useful insights. For this project, we will stick to options 1 and 2, which are essentially the same, as explained at the end of the next section, in which the derivation is continued using central moments.

### 3.5.4 Deriving a PDE for the second moment of mass using central moments

We now define the higher order moments of  $m$  to be

$$\langle m^n \rangle = \int_0^\infty (m - \langle m \rangle)^n \cdot f(x, y, m; t) dm,$$

which, instead of (29), leads to the integral

$$\int_0^\infty g(HC, m) f dm = HC \cdot g(HC, \langle m \rangle) + \frac{1}{2} \langle m^2 \rangle \frac{\partial^2 g}{\partial m^2}(HC, \langle m \rangle). \quad (32)$$

To get the equation for the second moment like (30), we will now not be multiplying by  $m^2$  before integrating over  $m$ , but by  $(m - \langle m \rangle)^2$ , to get:

$$\begin{aligned}
\frac{\partial \langle m(x, y, t)^2 \rangle}{\partial t} = & -\frac{\partial}{\partial x} \left[ \left( U(x, y) + \frac{1}{H(x, y)} \frac{\partial(H(x, y)D(x, y))}{\partial x} \right) \cdot \langle m(x, y, t)^2 \rangle \right] \\
& -\frac{\partial}{\partial y} \left[ \left( V(x, y) + \frac{1}{H(x, y)} \frac{\partial(H(x, y)D(x, y))}{\partial y} \right) \cdot \langle m(x, y, t)^2 \rangle \right] \\
& + \frac{\partial^2}{\partial x^2} [D(x, y) \cdot \langle m(x, y, t)^2 \rangle] + \frac{\partial^2}{\partial y^2} [D(x, y) \cdot \langle m(x, y, t)^2 \rangle] \\
& + 2 \int_0^\infty (m - \langle m \rangle) \cdot g(H(x, y, t)C(x, y, t), m) \cdot f(x, y, m; t) dm.
\end{aligned} \tag{33}$$

The last term is now simply given by

$$2 \int_0^\infty (m - \langle m \rangle) \cdot g(HC, m) f dm = 2 \langle m^2 \rangle \frac{\partial g}{\partial m}(HC, \langle m \rangle) + \langle m^3 \rangle \frac{\partial^2 g}{\partial m^2}(HC, \langle m \rangle). \tag{34}$$

To solve the closure problem, we can look at the three options provided in the previous derivation. Now option 1 and 2 are essentially the same: assuming the distribution of  $m$  is Gaussian directly implies that its third moment (the skewness) is zero, because the distribution is perfectly symmetrical. Filling in  $\langle m^3 \rangle = 0$  in (34) and (33) gives an equation that is solely dependent on  $\langle m^2 \rangle$ . We can solve for it, and plug the solution into equation (25), where we can solve for  $\langle m \rangle$ . With these two moments, and the assumption that our distribution is Gaussian, we have completely determined the distribution.

For now, let us assume that the distribution of  $m$  is indeed Gaussian as in options 1 and 2. In the following section, a solution for  $m$  and thus for the concentration is derived.

### 3.5.5 Solving the system for a Gaussian mass distribution

As discussed in the previous section, we can take the third central moment of  $m$  to be zero. Using this in (34) and plugging it into (33) gives the following equation for the second moment of  $m$ :

$$\frac{\partial \langle m^2 \rangle}{\partial t} = -\frac{\partial}{\partial x} [\tilde{U} \langle m^2 \rangle] - \frac{\partial}{\partial y} [\tilde{V} \langle m^2 \rangle] + \frac{\partial^2}{\partial x^2} [D \langle m^2 \rangle] + \frac{\partial^2}{\partial y^2} [D \langle m^2 \rangle] + 2 \langle m^2 \rangle \frac{\partial g}{\partial m}(HC, \langle m \rangle). \tag{35}$$

Using the product rule, this gives us

$$\begin{aligned}
\frac{\partial \langle m^2 \rangle}{\partial t} = & \langle m^2 \rangle \left[ -\frac{\partial \tilde{U}}{\partial x} - \frac{\partial \tilde{V}}{\partial y} + \frac{\partial^2 D}{\partial x^2} + \frac{\partial^2 D}{\partial y^2} + 2 \frac{\partial g}{\partial m}(HC, \langle m \rangle) \right] \\
& - \tilde{U} \frac{\partial \langle m^2 \rangle}{\partial x} - \tilde{V} \frac{\partial \langle m^2 \rangle}{\partial y} + D \left[ \frac{\partial^2 \langle m^2 \rangle}{\partial x^2} + \frac{\partial^2 \langle m^2 \rangle}{\partial y^2} \right].
\end{aligned} \tag{36}$$

Unfortunately, the first moment does appear once in this equation: in the evaluation of the derivative of the function  $g$ . So it forms a system with the equation for  $\langle m \rangle$ , which we already found when combining (25) and (32):

$$\begin{aligned}
\frac{\partial \langle m \rangle}{\partial t} = & \langle m \rangle \left[ -\frac{\partial \tilde{U}}{\partial x} - \frac{\partial \tilde{V}}{\partial y} + \frac{\partial^2 D}{\partial x^2} + \frac{\partial^2 D}{\partial y^2} \right] - \tilde{U} \frac{\partial \langle m \rangle}{\partial x} - \tilde{V} \frac{\partial \langle m \rangle}{\partial y} + D \left[ \frac{\partial^2 \langle m \rangle}{\partial x^2} + \frac{\partial^2 \langle m \rangle}{\partial y^2} \right] \\
& + HC \cdot g(HC, \langle m \rangle) + \frac{1}{2} \langle m^2 \rangle \frac{\partial^2 g}{\partial m^2}(HC, \langle m \rangle).
\end{aligned} \tag{37}$$

### 3.5.6 System of equations for a general function $g(HC, m)$

Putting together the three obtained equations, we get the following system from which we could solve  $\langle m \rangle$ . Note that these actually represent the zeroth, first and second moment of  $m$ :

- $$\frac{\partial(HC)}{\partial t} = \left[ -\frac{\partial\tilde{U}}{\partial x} - \frac{\partial\tilde{V}}{\partial y} + \frac{\partial^2 D}{\partial x^2} + \frac{\partial^2 D}{\partial y^2} \right] HC - \tilde{U} \frac{\partial(HC)}{\partial x} - \tilde{V} \frac{\partial(HC)}{\partial y} + D \frac{\partial^2(HC)}{\partial x^2} + D \frac{\partial^2(HC)}{\partial y^2}$$
- $$\begin{aligned} \frac{\partial\langle m \rangle}{\partial t} = & \left[ -\frac{\partial\tilde{U}}{\partial x} - \frac{\partial\tilde{V}}{\partial y} + \frac{\partial^2 D}{\partial x^2} + \frac{\partial^2 D}{\partial y^2} \right] \langle m \rangle - \tilde{U} \frac{\partial\langle m \rangle}{\partial x} - \tilde{V} \frac{\partial\langle m \rangle}{\partial y} + D \left[ \frac{\partial^2\langle m \rangle}{\partial x^2} + \frac{\partial^2\langle m \rangle}{\partial y^2} \right] \\ & + HC \cdot g(HC, \langle m \rangle) + \frac{1}{2} \langle m^2 \rangle \frac{\partial^2 g}{\partial m^2}(HC, \langle m \rangle) \end{aligned}$$
- $$\begin{aligned} \frac{\partial\langle m^2 \rangle}{\partial t} = & \langle m^2 \rangle \left[ -\frac{\partial\tilde{U}}{\partial x} - \frac{\partial\tilde{V}}{\partial y} + \frac{\partial^2 D}{\partial x^2} + \frac{\partial^2 D}{\partial y^2} + 2 \frac{\partial g}{\partial m}(HC, \langle m \rangle) \right] \\ & - \tilde{U} \frac{\partial\langle m^2 \rangle}{\partial x} - \tilde{V} \frac{\partial\langle m^2 \rangle}{\partial y} + D \left[ \frac{\partial^2\langle m^2 \rangle}{\partial x^2} + \frac{\partial^2\langle m^2 \rangle}{\partial y^2} \right] \end{aligned}$$

### 3.5.7 Finding a suitable function $g(HC, m)$

To solve the system of equations, we have to specify  $g(HC, m)$ . Here it is useful to think of some concrete functions  $g(HC, m)$  that behave as we would expect, based on the mass density, and the mass of the particle of interest. We would expect that if  $m$  is above a certain mass, it tends to fall apart and the mass decreases, where it will increase if it is below the certain mass. But the  $HC$  has some influence too: if it is high, the particle can easily interact with the lots of other particles around it, and its mass will increase. The opposite effect is true for a low  $HC$ .

If mass of the particle is very large, we expect it to shrink anyway, independent of  $HC$ . Such reasoning also applies to  $HC$ : if the density is very low, it is expected that the mass decreases, no matter what that mass is. Also, if  $HC$  is very high, the mass should increase. Summarized in a graph, the behavior in figure 1 is roughly what  $g$  is expected to show.

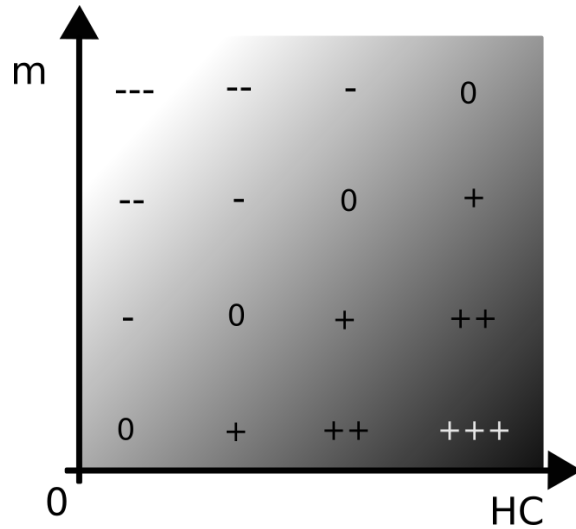


Figure 1. Expected sign and magnitude of  $g(HC, m)$  for various values of  $HC$  and  $m$ .

In general, an option for  $g$  could be

$$g(HC, m) = a(HC)^k - bm^l, \quad (38)$$

with  $a, b, k$  and  $l$  positive constants. The simplest version of this  $g$  would of course be the one with  $k = 1$  and  $l = 1$ :

$$g(HC, m) = aHC - bm. \quad (39)$$

Note that for this  $g$ , we did not even have to make the approximation using Taylor series, because all higher order derivatives are zero.

In our system of 3.5.6 there are three appearances of  $g$ , which we can now calculate:

$$\begin{aligned} g(HC, \langle m \rangle) &= aHC - b\langle m \rangle; \\ \frac{\partial g}{\partial m}(HC, \langle m \rangle) &= -b; \\ \frac{\partial^2 g}{\partial m^2}(HC, \langle m \rangle) &= 0. \end{aligned} \quad (40)$$

These might be different (more complicated) if we had chosen a less simple  $g$  than (39).

### 3.5.8 Final system of equations

Now, with all the assumptions and calculations, we get to a final system of equations to determine the distribution of  $m$ , presented below.

$$\begin{aligned} \bullet \quad \frac{\partial(HC)}{\partial t} &= \left[ -\frac{\partial \tilde{U}}{\partial x} - \frac{\partial \tilde{V}}{\partial y} + \frac{\partial^2 D}{\partial x^2} + \frac{\partial^2 D}{\partial y^2} \right] HC - \tilde{U} \frac{\partial(HC)}{\partial x} - \tilde{V} \frac{\partial(HC)}{\partial y} + D \left[ \frac{\partial^2(HC)}{\partial x^2} + \frac{\partial^2(HC)}{\partial y^2} \right] \\ \bullet \quad \frac{\partial \langle m \rangle}{\partial t} &= \left[ -\frac{\partial \tilde{U}}{\partial x} - \frac{\partial \tilde{V}}{\partial y} + \frac{\partial^2 D}{\partial x^2} + \frac{\partial^2 D}{\partial y^2} \right] \langle m \rangle - \tilde{U} \frac{\partial \langle m \rangle}{\partial x} - \tilde{V} \frac{\partial \langle m \rangle}{\partial y} + D \left[ \frac{\partial^2 \langle m \rangle}{\partial x^2} + \frac{\partial^2 \langle m \rangle}{\partial y^2} \right] \\ &\quad + a(HC)^2 - b\langle m \rangle HC \\ \bullet \quad \frac{\partial \langle m^2 \rangle}{\partial t} &= \langle m^2 \rangle \left[ -\frac{\partial \tilde{U}}{\partial x} - \frac{\partial \tilde{V}}{\partial y} + \frac{\partial^2 D}{\partial x^2} + \frac{\partial^2 D}{\partial y^2} - 2b \right] - \tilde{U} \frac{\partial \langle m^2 \rangle}{\partial x} - \tilde{V} \frac{\partial \langle m^2 \rangle}{\partial y} \\ &\quad + D \left[ \frac{\partial^2 \langle m^2 \rangle}{\partial x^2} + \frac{\partial^2 \langle m^2 \rangle}{\partial y^2} \right] \end{aligned}$$

Although the equation for  $\langle m^2 \rangle$  is still in this system, it is clear that it is not needed anymore: the equation for  $\langle m \rangle$  is only dependent on  $\langle m \rangle$  itself and  $HC$ , and the equation for  $HC$  is closed. Therefore, from the first and second equation,  $\langle m \rangle$  could be solved.

### 3.5.9 Comparison with currently used interaction equations

In [14], Winterwerp gives the following equation for the number concentration  $N$ , accounting for flocculation of cohesive sediment under the influence of turbulent shear:

$$\frac{\partial N}{\partial t} = -\alpha \frac{\partial N}{\partial x_i} + \beta \frac{\partial}{\partial x_i} \left( D \frac{\partial N}{\partial x_i} \right) - \gamma D^3 N^2 + \delta D^p N + \epsilon, \quad (41)$$

with  $\alpha, \beta, \gamma, \delta, \epsilon$  and  $p$  some parameters.

We notice that the number concentration  $N$  is equal to  $\frac{HC}{\langle m \rangle}$ . To get an equation for  $N$  from our final system of equations, we need to couple the equations for  $HC$  and  $\langle m \rangle$ :

$$\frac{\partial N}{\partial t} = \frac{\partial \left( \frac{HC}{\langle m \rangle} \right)}{\partial t} = HC \frac{\partial \left( \frac{1}{\langle m \rangle} \right)}{\partial t} + \frac{1}{\langle m \rangle} \frac{\partial(HC)}{\partial t} = -\frac{HC}{\langle m \rangle^2} \frac{\partial \langle m \rangle}{\partial t} + \frac{1}{\langle m \rangle} \frac{\partial(HC)}{\partial t}. \quad (42)$$

When only looking at the extra terms  $+a(HC)^2 - b\langle m \rangle HC$  from the second equation of our system, we get a contribution of

$$-\frac{HC}{\langle m \rangle^2} (a(HC)^2 - b\langle m \rangle HC) = -a \frac{(HC)^3}{\langle m \rangle^2} + b \frac{(HC)^2}{\langle m \rangle}$$

to (42). These are not completely similar to the extra terms in (41): an extra factor  $HC$  is added to both the negative and the positive term. Using our equations for  $HC$  and  $\langle m \rangle$ , it is not possible to give a closed equation for  $N$ . Without the factor  $HC$ , the terms would be in agreement with the ones in (41).

To be able to give a more accurate equation for  $N$ , we could change our choice of  $g$ . It appears that choosing

$$g(HC, m) = a - b \frac{m}{HC}$$

exactly gives the resulting terms  $-a \frac{(HC)^2}{\langle m \rangle^2} + b \frac{HC}{\langle m \rangle} = -aN^2 + bN$ .

It would be even better to base our choice of the function  $g(HC, m)$  on measurements. Then, we could possibly derive a closed equation for  $N$  with this new  $g$ . The derivation of an equation for  $\langle m \rangle$ , and thus  $N$ , as described in this section, could provide a physical and mathematical background for the equations that are currently used.

## 4 Numerical simulations of the various particle models

In this section, some particle models are used to do simulations, and the results are analyzed. To do the simulations, the random walk model and random flight model were implemented using MATLAB [2], with and without suspension, deposition and interaction. The numerical scheme used to approximate the solution of the SDEs is Euler-Maruyama. This is one of the most used schemes to approximate Itô SDEs [9].

The implementation was done by looping over many timesteps, and for each timestep, looping over each particle. In this last loop, the next position of the particle is determined, and, if applicable, other characteristics of the particle (such as its mass). The most important implementation aspects will be treated in the upcoming sections.

For all simulations, a domain of 20 by 20 was used ( $x \in [-10, 10]$  and  $y \in [-10, 10]$ ). The boundaries are treated by mirroring. This means that if a the new position of the particle would be outside the domain, we put the particle back at the same distance from the boundary, but inside the domain (as if the particle had bounced back from the boundary). For the flight model, the particle velocities are mirrored as well. Another option for treating the boundaries could have been that we see the domain as repeating: if a particle 'falls out' on the left, it comes back on the right of the domain. Mirroring was used instead, because it is more intuitive for the test cases described in section 4.1.

The used timestep in all simulations is 0.1, and for the random flight model, the values  $T_L = 1$  and  $\gamma = 1$  were used. This value for  $T_L$  implies that after, say,  $t = 20$ , or some comparable time, there should be no difference between the results of the random walk model and the random flight model. After some amount of Lagrangian timescales  $T_L$  have passed, the initial effects of the flight model should be no longer visible when compared to the results of the random walk model.

The various comparisons that will be made in this section are: between the random walk model and the random flight model (section 4.2), between the same two, including deposition and suspension (4.3), and between the random walk model with and without particle interaction (4.4). To make useful comparisons, three test situations are used. As said before, those are described in section 4.1.

Unless otherwise stated, figures in this chapter are made using MATLAB [2].

### 4.1 Test environments

Three test environments were used to test the implementation of the models and to analyze the results of the simulations. In each of the three environments, two of the functions  $H$ ,  $D$  and  $U$ ,  $V$  are taken constant, and for the other function, some profile is taken. Note that the functions are all assumed to be constant in time. These environments are partly equal to and partly based on the ones described by Heemink in [7].

#### 4.1.1 $H = 10$ , $U = V = 0$ , and $D$ a 2D Gaussian curve

In the first test environment, the water depth  $H$  is taken constant (10), and the water velocities are set to be absent. The diffusion coefficient  $D$  is varying in space. We take  $D$  to be a 2D Gaussian curve, plus some constant value. The specific function used is:

$$D(x, y) = 10 + 10 \exp(-0.03(x^2 + y^2)).$$

A plot of this function for the used domain is shown in figure 2.

It can be shown that after a long time, when some equilibrium has formed, the particle distribution over the domain should be uniform for this test case [7]. This is clear when looking at (7), and setting to zero the left hand side, and the  $U$  and  $V$  terms. With constant  $H$ , we get an equation

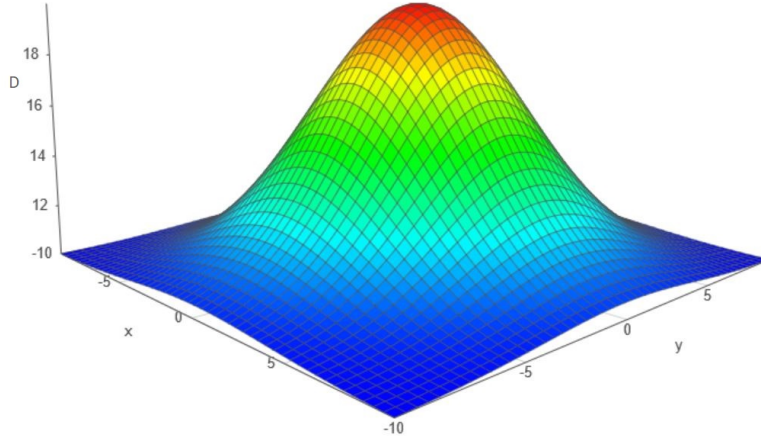


Figure 2. The function  $D(x, y)$ , used in the first test environment, with the values of  $D$  on the z-axis. Note that the lowest point of the curve is already at  $D = 10$ . Made using Academo [1].

of which a constant  $C$  is a solution. This is true for both the random walk and random flight model without any extra terms or equations. This prediction will be verified for the simulations in section 4.2.

#### 4.1.2 $U = V = 0$ , $D = 10$ , and $H$ a smooth curve with two levels

Now, for the second test environment, the water velocities are still absent, and  $D = 10$ .  $H$  is the function that will vary in space: the depth is greatest (20) for  $x$  around 0, and smallest (10) for  $x$  around  $-10$  and  $10$ . The function  $H$  is constant in  $y$ . The equation for  $H$  is taken to be

$$H(x, y) = 10 - 5 \tanh(x - 4) + 5 \tanh(x + 4).$$

A plot of the function is shown in figure 3.

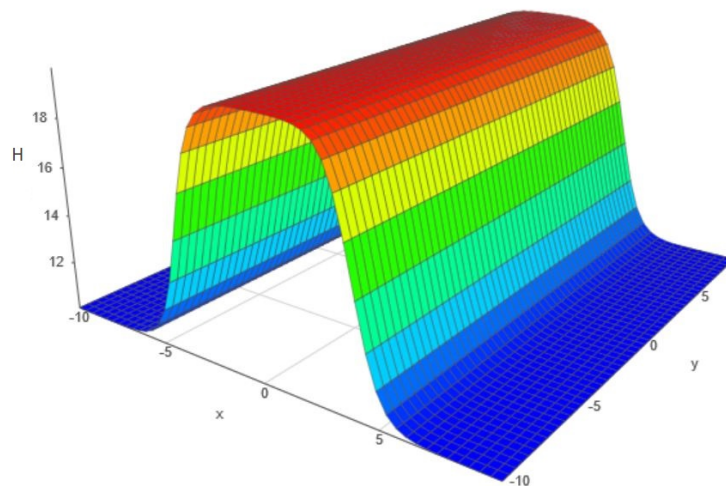


Figure 3. The function  $H(x, y)$ , used in the second test environment, with the values of  $H$  on the z-axis. Note that the height of the curve is at the lowest point at  $H = 10$ , and that the middle part is in fact deeper (greater  $H$  means deeper water). Made using Academo [1].

For longer simulation times, we expect that the depth-averaged concentration is equal over the whole domain. However, because we have a depth that is two times larger in the middle part of the domain, we expect twice as many particles there. The amount of particles is equal to the volume times concentration, and due to the depth being twice as large, the volume is also doubled. This long time behavior will as well be checked for the simulations in section 4.2.

### 4.1.3 $H = 10$ , $D = 10$ , and $U, V$ such that the water rotates divergence-free

The third and last test environment has constant  $D$  and  $H$ :  $H = 10$  and  $D = 10$ . We assume that the water is rotating clockwise in such a manner that the velocities perpendicular to the boundaries is zero. Otherwise we would notice an accumulation of particles near that border: bounced back from the boundary and pushed back again by the water velocity. Also we make the velocity field divergence-free. As a result, particles are not pushed away or towards the center by the water velocity.

The two used functions for  $U$  and  $V$  that form such a field are given below, and an impression of the vector field representing these velocities is shown in figure 4.

$$U(x, y) = \cos\left(\frac{\pi x}{20}\right) \sin\left(\frac{\pi y}{20}\right);$$

$$V(x, y) = -\sin\left(\frac{\pi x}{20}\right) \cos\left(\frac{\pi y}{20}\right).$$

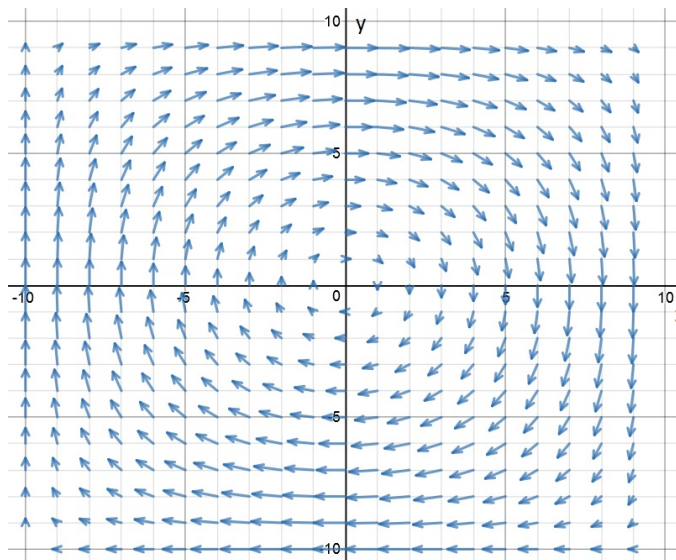


Figure 4. An impression of the vector field formed by the functions  $U(x, y)$  and  $V(x, y)$ , the water velocities in x- and y-direction respectively. These functions are used in the third test environment. Made using Desmos [3].

The long time behavior in this test case should again be such that the final particle distribution is uniform. As Heemink points out in [7], it is important that the water velocity is integrated analytically or that the numerical integration method uses a very small timestep. Otherwise, numerical errors can induce divergence in the model, pushing the particles away (or towards) the center of the domain. As this is not the desired behavior, the functions are evaluated analytically in the implementation of the models described in this report.

## 4.2 Random walk model & random flight model

In this section, the results of a particle simulation for both the random walk model and the random flight model are shown. In these models, no extra terms or equations are added: deposition, suspension, and particle interaction are treated in the upcoming sections.

For the simulations in this section, 500 particles were simulated. For test case 1 and 2, all had position  $(x, y) = (0, 0)$  at  $t = 0$ , as for example can be seen in the first plot of figure 5 and 6. In the flight model simulation, also the initial velocities of all particles were set to zero. For test case 3, only the starting position of the particles is slightly different.

### Test case 1

First, it is interesting to look at the first timesteps of the simulation, where the particles spread out from the middle of the domain. In figures 5 and 6, we can immediately see the difference between the random walk model and the random flight model. These simulations were done in test environment 1.

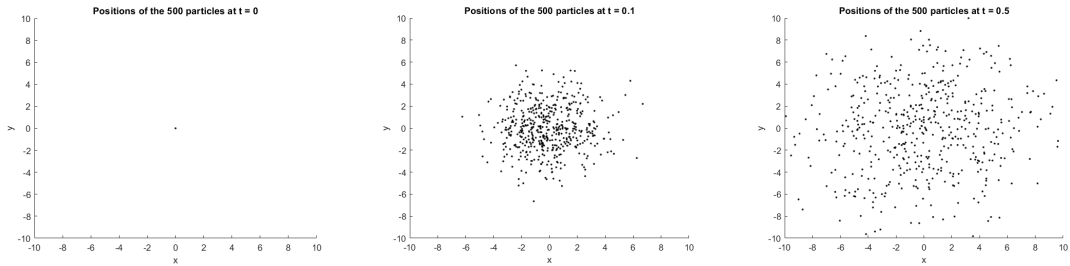


Figure 5. Results of a simulation of 500 particles in test environment 1, using the random walk model, at some small values of  $t$ .

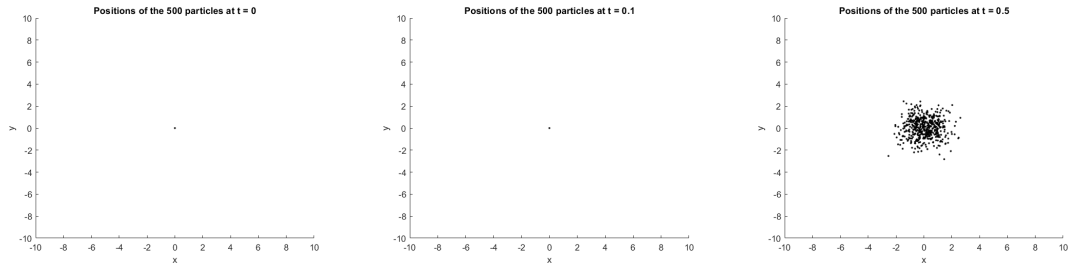


Figure 6. Results of a simulation of 500 particles in test environment 1, using the random flight model, at some small values of  $t$ .

In these figures, we can clearly see that the particles in the random flight model need to 'start up': they start with zero turbulent velocity, and it takes time to change those velocities. Because the water velocity is zero and the diffusion gradient is nearly zero as well around the middle of the domain, the only term in the flight model (10) that causes displacement during the first timesteps is  $\sigma U_t dt$  (and  $\sigma V_t dt$  for the  $y$ -direction). It takes time for  $U_t$  and  $V_t$  to change from zero to a significant velocity. The result after one timestep, at  $t = 0.1$ , in figure 6 is as expected. In the first step, the particles have zero velocity, so their positions do not change. Only their velocities change, which gives changes in position for the second timestep. From then on, the positions can change.

Then, for larger  $t$ , we get the results as shown in figures 7 and 8.

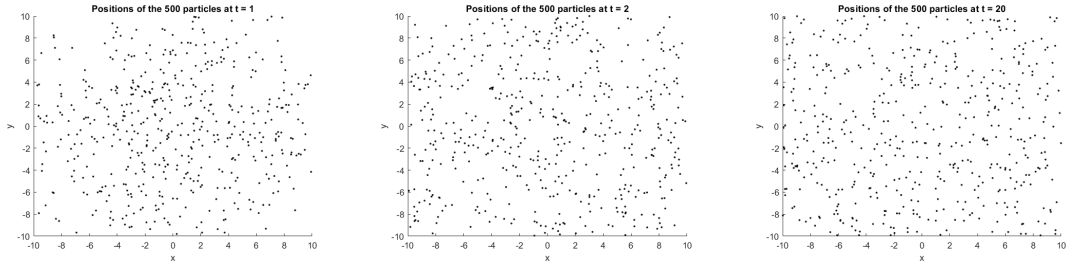


Figure 7. Results of a simulation of 500 particles in test environment 1, using the random walk model, at some larger values of  $t$ .

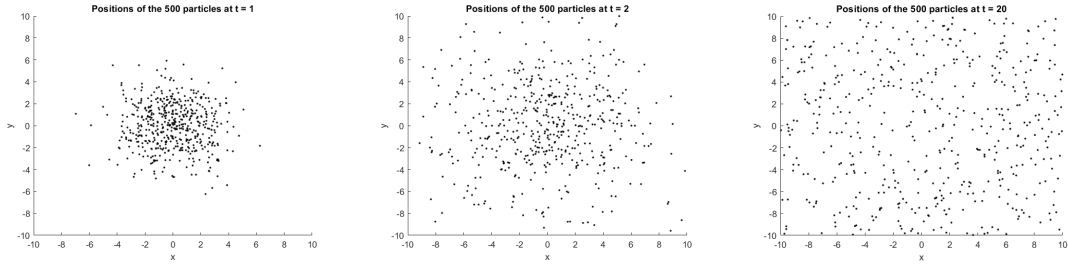


Figure 8. Results of a simulation of 500 particles in test environment 1, using the random flight model, at some larger values of  $t$ .

As expected, the particles seem to be uniformly distributed over the domain. To make this even clearer, a histogram of the distance of the particles to the center of the domain is shown for both models in figure 9. These histograms can be made because our conditions are completely rotation symmetric. For test case 3, we also have this rotational symmetry, and we can produce the same type of histograms.  $r$  is not taken larger than 10, because from then, the left, right, upper and lower boundaries are touched. And indeed, the particle distributions seem uniform.

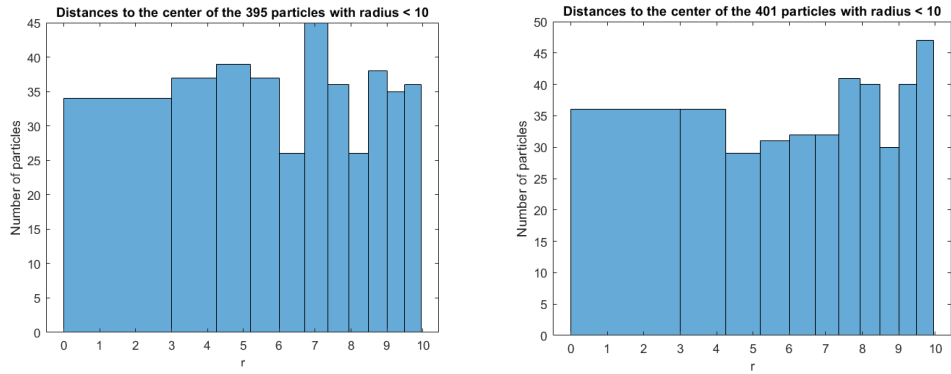


Figure 9. Histograms of the distance  $r$  of the particles to the center of the domain at  $t = 20$ , for the random walk model (left) and flight model (right), in test case 1. The bins are chosen such that each represents an equal area of the domain.

## Test case 2

The same starting conditions apply to the simulations in test environment 2. The results of the simulation for both the random walk and the random flight model are shown in figure 10.

As expected, the particles are more concentrated in the middle part of the domain than in the outer parts. To compare the number of particles, a histogram can be made for the absolute  $x$ -positions

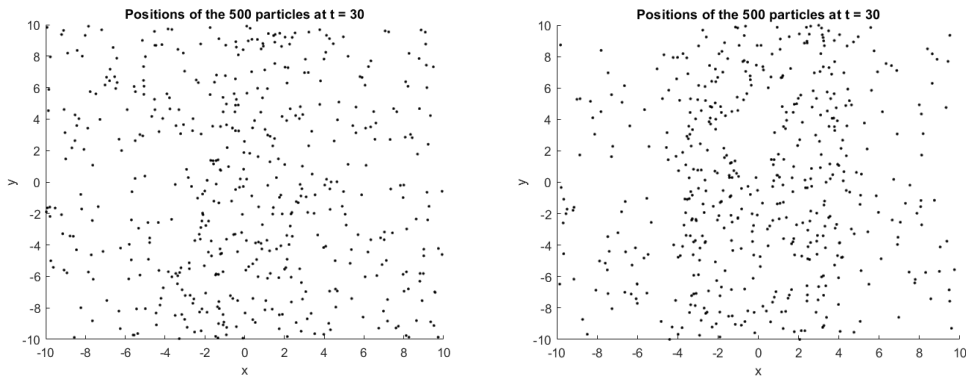


Figure 10. Results of a simulation of 500 particles in test environment 2, using the random walk model (left) and flight model (right), at  $t = 30$ .

of the particles. These are shown in figure 11.

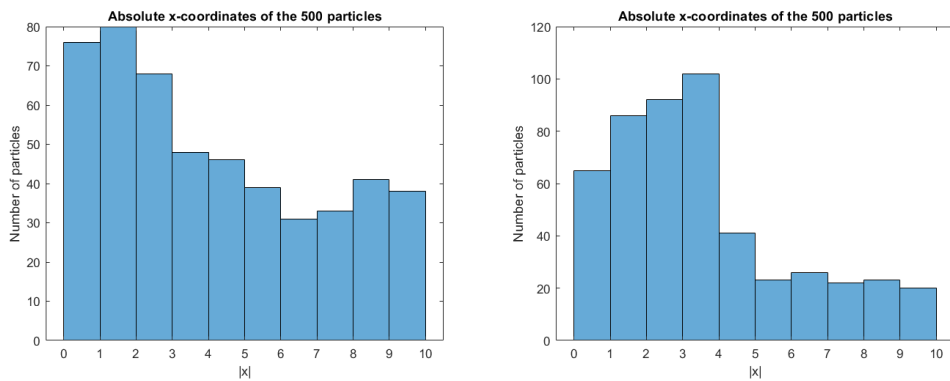


Figure 11. Histograms of the absolute x-position  $|x|$  of the particles at  $t = 30$ , for the random walk model (left) and flight model (right), in test case 2.

Indeed, it is visible that for both models, more particles are present in the middle area. However, we expected about twice as many particles in this area than in the outer areas. This is approximately true for the walk model. But it appears that, for the flight model, this ratio is much larger (4:1 instead of 2:1).

Taking a smaller value for  $T_L$  (0.1 instead of 1) gives results as expected, even for a smaller time  $t = 20$ . Those are shown in figure 12. This confirms the statement that the random flight model acts more like the random walk model for smaller  $T_L$ .

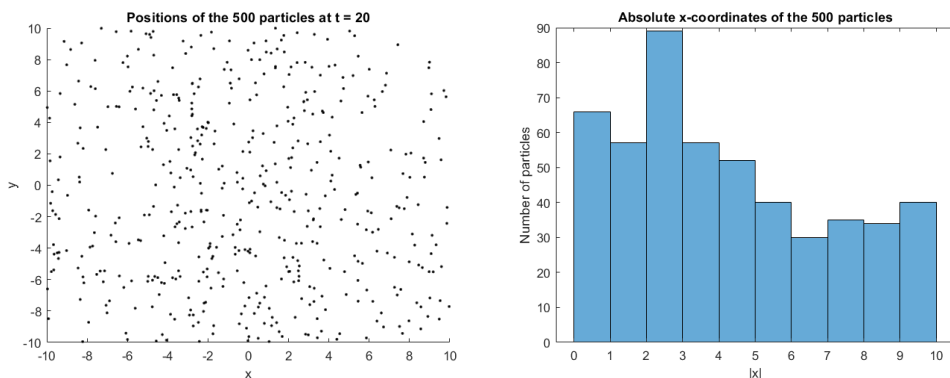


Figure 12. Results of a simulation and a histogram for the absolute x-position  $|x|$  of the simulated particles at  $t = 20$ , for the random flight model in test case 2.

### Test case 3

For test environment 3, it is again interesting to have a look at the beginning of the simulation, when particles start to spread and are moved by the water. We now let the particles start in the point  $(5, 0)$ , so that we can see the particles flow in the clockwise direction due to the water flow. This behavior is shown for the random walk model in figure 13.

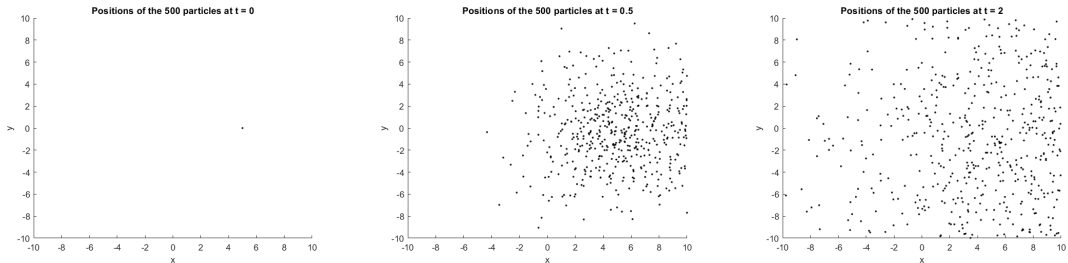


Figure 13. Results of a simulation of 500 particles in test environment 3, using the random walk model, at some small values of  $t$ .

Just as in test case 1, the result should be a uniform distribution for both models. The simulation results at the large value  $t = 20$  are shown in figure 14.

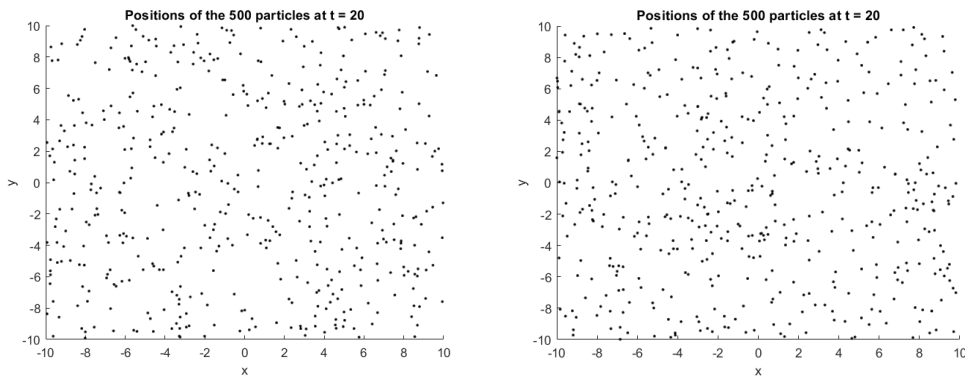


Figure 14. Results of a simulation of 500 particles in test environment 3, using the random walk model (left) and flight model (right), at  $t = 20$ .

To check if these distributions are indeed approximately uniform, again two histograms can be made for both models at  $t = 20$ . These are shown in figure 15, where it is clear that the expectations are met.

### 4.3 Random walk model & random flight model with deposition and suspension

The implementation of deposition and suspension was already extensively discussed in sections 3.3 and 3.4. An important note, which was not yet mentioned, is that after a particle is deposited, the simulation ignores it for the rest of the time. It is assumed that the bottom of the water has an infinite amount of particles on it, so that it does not matter for suspension whether there are more or fewer particles deposited at some position.

For the tests with both models including deposition and suspension, the starting point was 900 particles in a  $30 \times 30$  grid, as can be seen in the left plot of figures 17 and 18. Furthermore, testing environment 3 was used, with a small change: to speed up the forming of some equilibrium a bit, the water velocities were taken 3 times larger:

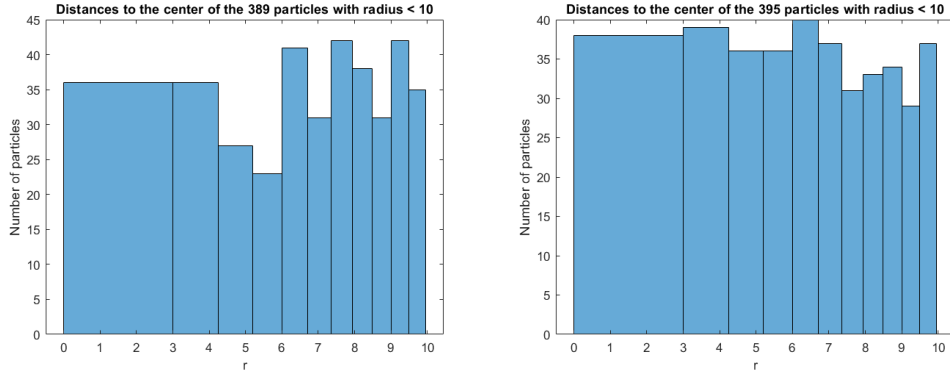


Figure 15. Histograms of the distance  $r$  of the particles to the center of the domain at  $t = 20$ , for the random walk model (left) and flight model (right) in test case 3. The bins are chosen such that each represents an equal area of the domain.

$$U(x, y) = 3 \cos\left(\frac{\pi x}{20}\right) \sin\left(\frac{\pi y}{20}\right) ;$$

$$V(x, y) = -3 \sin\left(\frac{\pi x}{20}\right) \cos\left(\frac{\pi y}{20}\right) .$$

Furthermore, for deposition,  $\epsilon = 0.5$  was taken, and for suspension,  $\frac{\lambda_s}{M_p} = 0.25$ .

During several timesteps, some particles were suspended, and were thus added to the total number of particles, and some particles in suspension were deposited. After some time, an equilibrium in particle number will be established: the total number of particles in suspension remains approximately the same. This is because the number of suspended particles each timestep is independent of time (because  $U$ ,  $V$  and the other parameters for suspension are), and thus by approximation constant. The number of deposited particles is approximately a constant times the total number of particles in suspension. For a certain number of particles, these values cancel out, and we have about the same number for all following timesteps. Based on observations for shorter simulations, this value was estimated to be approximately 900 for the specific conditions in the adapted testing environment 3. So starting at 900 particles, we expect to approximately keep that same value of particles in suspension during the simulation.

The resulting water speed squared ( $U^2 + V^2$ ) at every position of the domain is shown in figure 16. Because particle suspension is only dependent on constants and this exact term, we expect that most particles are suspended in the side areas of the domain, and less in the middle and corners. Particle deposition is not dependent on position, and therefore the expectation is that after some time, more particles will be present in the side areas.

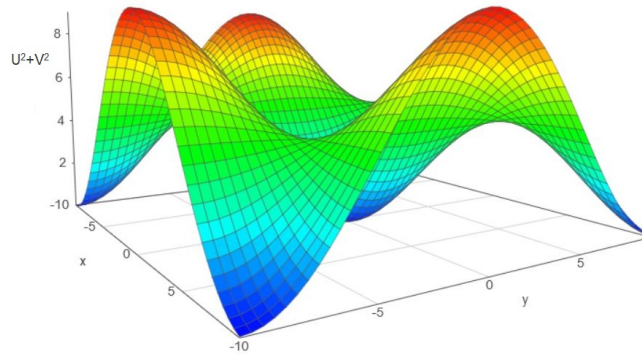


Figure 16. The water speed squared ( $U^2 + V^2$ ) on the  $z$ -axis, for every position  $(x, y)$  in the domain. Made using Academo [1].

In figures 17 and 18, some results of the simulations are shown. Indeed, the particle number stays approximately constant around 900. It is also clear that there are more particles present on the sides, as expected. This effect is also visible in figure 19, a map with all deposited particles. Of course, if more particles are present in an area during the simulation, and each particle is equally likely to be deposited, the same kind of distribution is obtained. The suspension effects are the same for both models, as  $U$  and  $V$  are the same. The random walk and random flight models seem to give similar results, as we would expect. There is not much of an initial difference between them, because we now started with a uniform distribution of particles. Therefore, also the deposition map is largely the same.

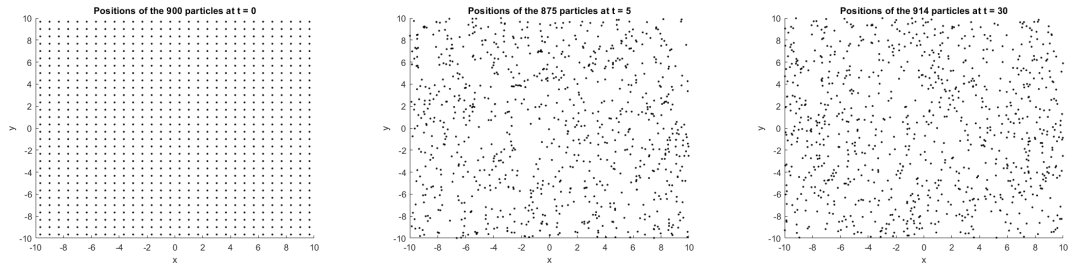


Figure 17. Results of a simulation that begins with 900 particles in an adapted test environment 3, using the random walk model, including deposition and suspension, at some small values of  $t$ .

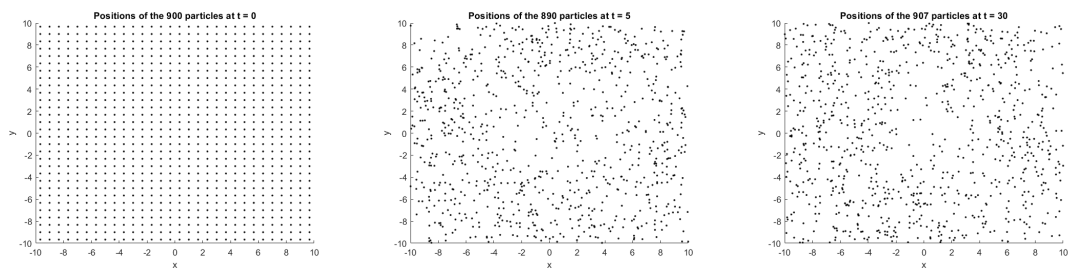


Figure 18. Results of a simulation that begins with 900 particles in an adapted test environment 3, using the random flight model, including deposition and suspension, at some small values of  $t$ .

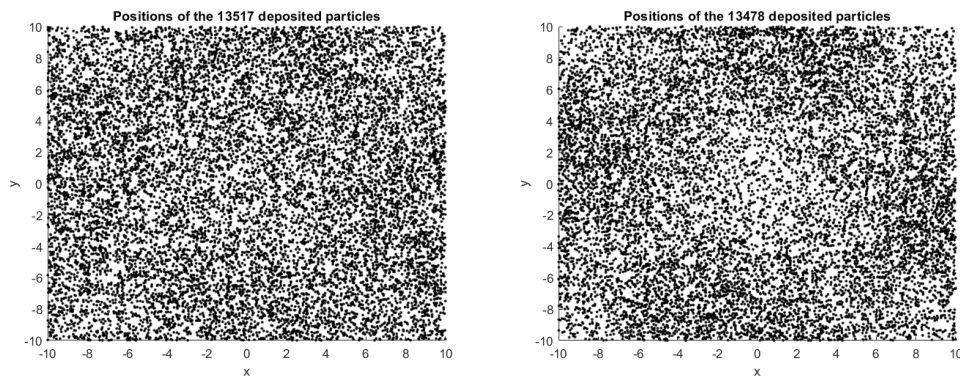


Figure 19. Position of all deposited particles during a simulation that started with 900 particles and lasted until  $t = 30$ , in an adapted test environment 3, using the random walk model (left) and flight model (right), including deposition and suspension.

To check if the particle distributions are really as explained, again histograms can be made. For the walk and flight model at  $t = 30$ , these are shown in figure 20. Indeed, the particles are not uniformly distributed, but there are more particles far away from the center than near it. In the deposition maps, it is even visible with the naked eye that there are more deposited particles in high speed areas, with some deviation in clockwise direction due to the flow direction.

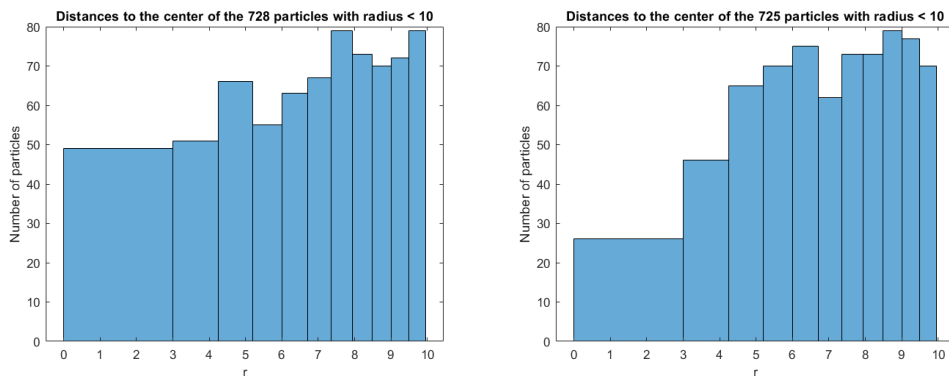


Figure 20. Histograms of the distance  $r$  of all particles to the center of the domain at  $t = 30$ , for the random walk model (left) and flight model (right), including deposition and suspension. The bins are chosen such that each represents an equal area of the domain.

That the deposition map of the random flight model has areas that are more clearly defined, is probably because of the particles having to 'start up', and therefore staying more on the sides. Although they are effected the same by the water flow as in the random walk model, their turbulent velocities are initially zero. Therefore, they do not spread out as quick as in the walk model.

Particles get suspended more in the outer areas of the domain with zero initial velocity. In the flight model, they stay around their initial position longer than in the walk model (such as visible in figures 5 and 6). Therefore, the particles are in the side areas for a longer period of time, and thus have more chance to be deposited there again.

#### 4.4 Random walk model without & with particle interaction

The implementation of particle interaction is somewhat more complex than that of deposition and suspension. We now have to track not only position, but also mass of the particles. Each timestep, we have to calculate the change in mass for each particle, based on its own mass and the mass density at the position of the particle. This density is a measure for how many particles are present in the same area as the particle of interest. In the implementation, it is determined using the positions of the other particles around it. This can be done using a kernel estimation, of which an illustration is shown in figure 21, for 14 particles.

This kernel estimation is made by constructing for each particle a 3D surface around the position of that particle, and adding all those curves together to form an approximation of the concentration at each position. If there are lots of particles around some position, the distribution has a peak at that position, and the density  $HC$  is therefore estimated to be large, as can be seen in figure 21. Note that in the actual simulations, 500 particles are used, and the estimated surface is way smoother, with fewer gaps between peaks, than in this figure.

For this comparison, different starting positions were used: 225 particles started in a 15x15 grid, and 25 more particles were released at  $(0, 0)$ . This was done to show the effect of the high mass density in the middle of the domain. In figure 22, some results of the simulation are shown. The mass growth of the particles in the middle is immediately visible. After several timesteps, these heavy particles are spread out a bit, which lowers  $HC$  in that area. This makes those particles shrink in mass again.

An effect that is visible in the whole domain is that regions with many particles tend to have particles with large masses in them. This makes sense, because as explained before, many particles give a large  $HC$  and thus larger values of  $g$  and  $dM$ .

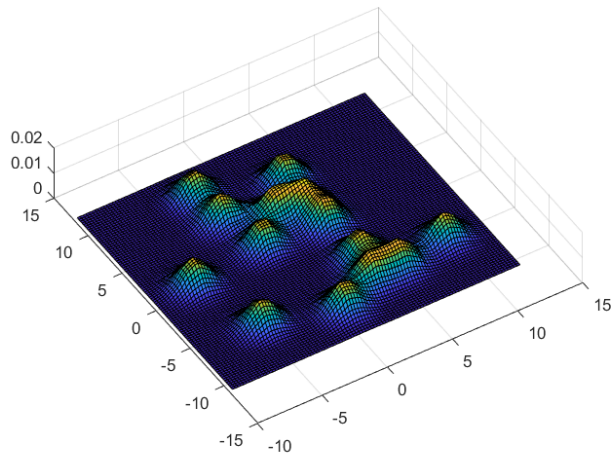


Figure 21. An example of a kernel estimation of  $HC$  for 14 particles.

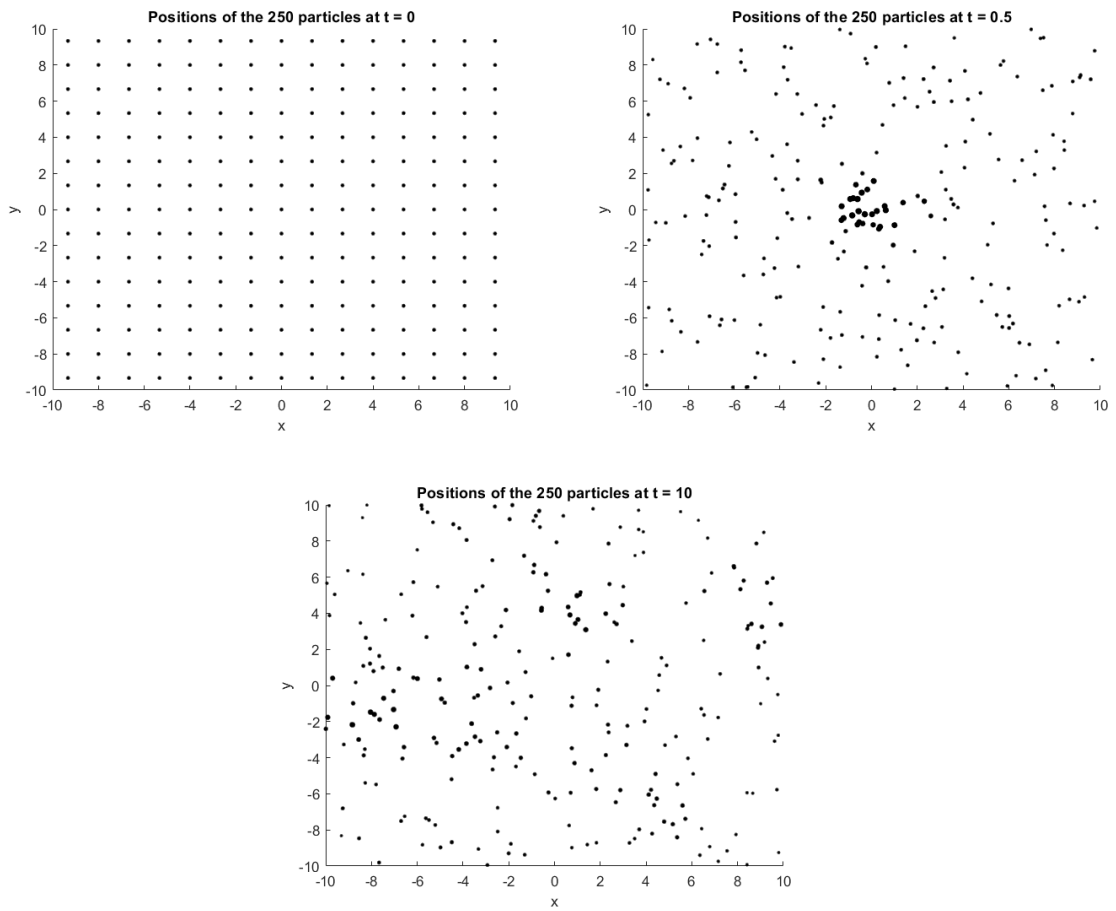


Figure 22. Results of a simulation of 250 particles in test environment 3, using the random walk model including interaction, for three values of  $t$ . Larger dots represent particles with greater mass.

## 5 Conclusions and recommendations

In this thesis, the random walk model and random flight model were modified to account for particle suspension, deposition and interaction. These models were analyzed and various simulations were done. From the different analyses, several conclusions can be drawn. Also, some recommendations for follow-up research are given.

### Conclusions

Without any additions, the difference between the two models is in the initial stage: the random flight model keeps track of the turbulent velocities of particles, and if we start with particles that have zero initial velocity, it takes time to accelerate them. Therefore, the particles initially do not move much if there is no water flow or diffusion or height gradient. The random walk model, in contrary, always displaces the particles in the same way, and does not take initial acceleration into account. As a result, the particles start to move quicker than in the flight model. This behavior is clearly visible in the simulations. For large times, the flight model becomes approximately equal to the walk model, and the results are the same. For various test conditions, the implementation of the model was verified, and the results turned out to be as expected.

Deposition can be implemented in the walk and flight model by adding for each particle a probability that it is deposited during the current timestep. In the advection-diffusion equation, this effect can be described by a sink term, and the models are both consistent with the new equation. Suspension is a source term in the advection-diffusion equation, and to get a particle model that is consistent with this equation, it is possible to add suspension to it by calculating per grid cell how many particles should be suspended, based on the water speed in that cell. With this model, the results of simulations show that in areas with high water speed, more particles are present, and thus more particles are deposited over time. In this effect, there is not much difference between the random walk and random flight model.

Finally, to account for particle interaction, a new equation can be added to the random walk model. This continuous equation describes the difference in mass that a particle experiences after each timestep, due to interaction with other particles, or falling apart itself. With several assumptions and approximations, a system of partial differential equations for the final mass distribution can be obtained. In the simulations, it turns out that particles are heavier in areas where relatively many particles are present, and lighter in other regions. However, this difference in mass only depends on the distribution of particles, and not on position.

For the basic random walk model and random flight model, the corresponding partial differential equation is the well known advection-diffusion equation. For deposition and suspension, two extra source terms are added. When extending the random walk model with particle interaction, the equation obtained is not in complete agreement with the one that is currently used. This is due to the choice of the function for particle mass that was described in the previous paragraph. A logical next step would be to base the choice of this function on measurements. The resulting equation could then again be analyzed and compared to the currently used equation.

### Recommendations

One of the recommendations for follow-up research would be to do simulations in a domain with a more realistic shape and more realistic conditions. A different shape could give rise to interesting effects, and it is a challenge to implement particle behavior at borders that are not as smooth as the ones in this project. Different conditions include more complex water velocities and time-varying depth and water velocities (think of the tides). As every single condition in this thesis was constant in time, implementing time dependency would cover some aspects that were not treated during this project.

Of course, the model for interaction could be chosen differently. For the sake of this project, and the goal to compare the currently used concentration equations to the ones obtained now, a continuous equation for the mass change was taken. This way, the Fokker-Planck equation could be used. A different choice for a mass change model could be a discrete one, in which two particles are actually bound together and their mass adds up. Also, the choice for an interaction model could be based on measurements.

It would be interesting to see the effects of the different particle masses on other particle behavior, such as deposition: heavy particles tend to be deposited faster than light ones. In this project, only the isolated effects of particle interaction were studied.

The real strength of the described models will only become clear after some more research is done. To describe real-world phenomena, more realistic conditions should be explored, and the model for particle interaction could be improved and integrated in other models.

## References

- [1] 3D Surface Plotter, Academo. <https://academo.org/demos/3d-surface-plotter> .
- [2] MATLAB and Statistics Toolbox Release 2017b, The MathWorks, Inc., Natick, Massachusetts, United States.
- [3] Vector Field Generator, Desmos. <https://www.desmos.com/calculator/eijhparfmd> .
- [4] CHARLES, W.M. *Transport modelling in coastal waters using stochastic differential equations*. 2007.
- [5] FISCHER, H.B., LIST, E.J., KOH, R.C.Y., IMBERGER, J., & BROOKS, N.H. *Mixing in inland and coastal waters*. Academic Press, New York, 1979.
- [6] FREEDMAN, D. *Brownian Motion and Diffusion*. Holden-Day Inc., San Fransisco, 1971.
- [7] HEEMINK, A.W. Stochastic modelling of dispersion in shallow water. *Stochastic Hydrology and Hydrolics*, 4 (1990), 161–174.
- [8] HEEMINK, A.W. *Numerical Methods for Stochastic Differential Equations (Course notes WI4260TU)*. 2017.
- [9] IACUS, S.M. *Simulation and Inference for Stochastic Differential Equations*. Springer-Verlag, New York, 2008.
- [10] MIEDEMA, S.A., & RAMSDELL, R.C. Hydraulic transport of sand/shell mixtures in relation with the critical velocity. *Terra et Aqua*, 122 (2011), 18–27.
- [11] VAN DEN AKKER, H., & MUDDER, R. *Fysische transportverschijnselen*. Delft Academic Press, Delft, 1996.
- [12] VAN STIJN, TH. L., PRAAGMAN, N., & VAN EIJKEREN, J. Positive advection schemes for environmental studies. *In: Numerical methods in laminair and turbulent flow*. Taylor, C. et al. (ed.), Pineridge Press, Swansea (1987), 1256–1267.
- [13] VERNEY , R., LAFITE, R., BRUN-COTTAN, J. C., & LE HIR, P. Behaviour of a flocculation population during a tidal cycle: Laboratory experiments and numerical modelling. *Continental Shelf Research*, 31 (2011), S64–S83.
- [14] WINTERWERP, J.C. On the flocculation and settling velocity of estuarine mud. *Continental Shelf Research*, 22 (2002).

## Appendix: Third non-central moment of the normal distribution

We know that the third (and above) central moment of the normal distribution is zero. So we get

$$\begin{aligned} 0 &= \langle (m - \langle m \rangle)^3 \rangle = \langle m^3 - \langle m \rangle^3 - 3\langle m \rangle m^2 + 3m\langle m^2 \rangle \rangle \\ &= \langle m^3 \rangle - \langle m \rangle^3 - 3\langle m \rangle \langle m^2 \rangle + 3\langle m \rangle \langle m \rangle^2 \\ &= \langle m^3 \rangle - 3\langle m \rangle \langle m^2 \rangle + 2\langle m \rangle^3 \end{aligned} \tag{43}$$

which gives us

$$\langle m^3 \rangle = 3\langle m \rangle \langle m^2 \rangle - 2\langle m \rangle^3 \tag{44}$$